Chowdry, V., & Westheimer, F. H. (1979) *Annu. Rev. Biochem. 48*, 293–325.
Covey, D. F., & Robinson, C. H. (1976) *J. Am. Chem. Soc. 98*, 5038–5040.
Dixon, M. (1953) *Biochem. J. 55*, 170–171.
Einstein, A. (1908) *Z. Elektrochem. 14*, 235.
Giannini, M., & Fedi, M. (1960) *Boll. Chim. Farm. 99*, 24–26.
Godeau, J. F., Schorderet-Slatkine, S., Hubert, P., & Baulieu, E. E. (1978) *Proc. Natl. Acad. Sci. U.S.A. 75*, 2353–2357.
Gosting, L. J. (1956) *Adv. Protein Chem. 11*, 442–445.
Inman, J. (1974) *Methods Enzymol. 34*, 30–58.
Jarabak, R., Colvin, M., Moolgavkar, S. H., & Talalay, P. (1969) *Methods Enzymol. 15*, 642–651.
Kawahara, F. S., Wang, S. F., & Talalay, P. (1962) *J. Biol. Chem. 237*, 1500–1506.
Mäkinen, K. K., & Mäkinen, P. (1982a) *Photochem. Photobiol. 35*, 761–765.
Mäkinen, K. K., & Mäkinen, P. (1982b) *Eur. J. Biochem. 123*, 171–178.
Martyr, R. J. (1974) Ph.D. Thesis, University of California, Davis, Davis, CA.
Martyr, R. J., & Benisek, W. F. (1973) *Biochemistry 12*, 2172–2178.
Means, G. E., & Feeney, R. E. (1971) *Chemical Modification of Proteins*, pp 165–169, Holden-Day, Inc., San Francisco.
Nakai, N., Lai, C. Y., & Horecker, B. L. (1974) *Anal. Biochem. 58*, 563–570.
Ogez, J. R., Tivol, W. F., & Benisek, W. F. (1977) *J. Biol. Chem. 253*, 6151–6155.
Penning, T. M., & Talalay, P. (1981) *J. Biol. Chem. 256*, 6851–6858.
Penning, T. M., Covey, D. F., & Talalay, P. (1981) *J. Biol. Chem. 256*, 6842–6850.
Pollack, R. M., Kayser, R. H., & Bevins, C. L. (1979) *Biochem. Biophy. Res. Commun. 91*, 783–790.
Rubenstein, M., Shechter, Y., & Patchornik, A. (1976) *Biochem. Biophys. Res. Commun. 70*, 1257–1263.
Sadler, S. E., & Maller, J. L. (1982) *J. Biol. Chem. 257*, 355–361.
Shechter, Y., Rubinstein, M., & Patchornik, A. (1977) *Biochemistry 16*, 1424–1430.
Singh, P., Lewis, S. D., & Shafer, J. A. (1979) *Arch. Biochem. Biophys. 193*, 284–293.
Voss, H. F., Ashani, Y., & Wilson, I. B. (1974) *Methods Enzymol. 34*, 581–591.
Willis, A. T. (1969) *Methods Microbiol. 3B*, 86–87.

Kinetics of RNA Replication†

Christof K. Biebricher, Manfred Eigen, and William C. Gardiner, Jr.*

ABSTRACT: The reaction kinetics of single-stranded RNA replication were investigated by means of analytical and computer simulation methods. A model reaction mechanism is proposed that is in accord with the extensive experimental data available for the replication of various templates by the enzyme Qβ replicase. Despite the complexity of this mechanism, conventional concepts of steady-state and dynamic enyzme catalysis and plausible values of the rate and stability constants for the elementary reactions suffice to provide detailed understanding of RNA replication kinetics. The main features can be described with simple formulas that are analogous to traditional descriptions of enzyme kinetics.

Self-reproduction is the basis of genetic information transfer and thus also of natural selection and evolution. Indeed, the earliest self-reproductive systems able to organize themselves in a selective fashion were most likely composed of short single-stranded RNA molecules (Eigen, 1971). It is therefore especially interesting to study the mechanism of single-stranded RNA replication. The detailed mechanism of the autocatalytic growth process that occurs for self-replicating RNA molecules, i.e., for RNA species whose plus and minus strands can both the replicated by the same enzyme, is important for their selection and evolution.

However, while the kinetics of enzyme catalysis have been studied in great detail and for a broad variety of reactions since the subject was given its theoretical foundation by Michaelis and Menten in 1913, enzyme-catalyzed, template-instructed polymerization reactions have had little attention from kineticists. This is due in part to the intrinsic mechanistic complexity of polymerization reactions and in part to the difficulty of finding a suitable prototype reaction for experimental studies. The latter problem has now been solved by the establishment of the reaction mechanism of the in vitro replication of suitable RNA strands by the enzyme Qβ replicase. A theoretical analysis of the reaction mechanism of RNA replication based upon the available experimental results is presented in this paper.

Experimental Background

The first replication system to be studied in vitro was the replication of RNA-containing bacteriophages. In contrast to the long-known RNA-containing plant viruses like TMV, whose replication mechanism is still unclear (Hirth & Richards, 1981), several groups succeeded shortly after the discovery of RNA-containing bacteriophages (Loeb & Zinder, 1961) in detecting RNA synthesis in cellular extracts of infected cells (Haruna et al., 1963; Weissmann et al., 1963a,b; August et al., 1963). An enzyme that specifically amplified viral RNA while ignoring host RNA was partially purified from infected cells (Haruna et al., 1963; Spiegelman & Doi, 1963) and called RNA replicase (Spiegelman & Hayashi, 1963). The replicase of phage Qβ proved to be a relatively stable enzyme and was therefore adopted for most in vitro experiments (Haruna & Spiegelman, 1965a,b). Spiegelman et al. (1965) showed that the product of in vitro replication

† From the Max-Planck-Institut für Biophysikalische Chemie, D-3400 Göttingen, Federal Republic of Germany (C.K.B. and M.E.), and the Department of Chemistry, University of Texas, Austin, Texas 78712 (W.C.G.). *Received December 15, 1982.* This research was carried out under the auspices of the Max-Planck-Gesellschaft. Additional support from the Alexander von Humboldt, Fritz Thyssen, and Robert Welch Foundations is also acknowledged.

0006-2960/83/0422-2544$01.50/0

is infective viral RNA and Pace & Spiegelman (1966) showed that the replication is template instructed. Replication of viral RNA leads first to the production of a complementary minus strand (Weissmann & Feix, 1966), often found in vitro to be associated with the viral strand to form a Watson–Crick RNA double helix (Mills et al., 1966) also present in infected cells (Kaerner & Hoffmann-Berling, 1964; Kelly & Sinsheimer, 1964, 1967; Ammann et al., 1964). The synthesized Qβ minus strand is also a very effective template (Feix et al., 1967, 1968; Weissmann & Feix, 1966) for Qβ replicase; up to five plus strands can be synthesized simultaneously on one minus strand (Franklin, 1966; Weissmann, 1974). Synthesis of plus and minus strands was demonstrated to proceed by incorporation of nucleoside triphosphates in the 5′ to 3′ direction (Banerjee et al., 1967; August et al., 1968). the active template and the product of replication were found to be single-stranded plus and minus Qβ RNA (Weissmann et al., 1968), which easily anneal to the fully double-stranded Hofschneider structure (Ammann et al., 1964; Kaerner & Hoffmann-Berling, 1964) or the partially double-stranded Franklin structure (Franklin, 1966; Spiegelman et al., 1968). The synthesis of the Qβ minus strand requires the participation of a host factor in addition to the Qβ replicase (Hori et al., 1967; August et al., 1968; Spiegelman et al., 1968). The advantage of the host factor in the Qβ infection system is probably the provision for almost exclusive synthesis of viral strands late in the infection process (Fedoroff, 1975).

Despite the high in vivo specificity of Qβ replicase, a large number of so-called nonphysiological templates are also accepted by Qβ replicase in vitro. This circumstance has provided much insight into the replication mechanism. The term "nonphysiological" refers to the fact that the enzyme was selected during evolution for recognizing only its cognate RNA and ignoring other possible templates. The replicase function itself, however, must be quite similar or identical for all templates.

Poly(C) and cytidylate-rich nucleotide copolymers are templates of Qβ replicase; however, the product of synthesis is the double strand of the template and its replica (Hori et al., 1967; Eikhom & Spiegelman, 1967). Furthermore, after one round of replication, the replicase cannot be recycled. Qβ replicase can synthesize replica copies of a variety of templates if its specificity is altered or circumvented by special conditions. The simplest way is to add a complementary oligonucleotide as primer in addition to the template (Feix & Hake, 1975; Feix, 1976). Like most polymerases, the Qβ replicase is able to elongate the primer. Another way to induce synthesis of the complementary strand is to trigger initiation of replication by using high concentrations of GTP (Blumenthal, 1980) and/or Mn^{2+} ions (Palmenberg & Kaesberg, 1974; Obinata et al., 1975). A third way to obtain replica synthesis is to add a stretch of C residues to the 3′ end of a template (Feix & Sano, 1975). Unfortunately, in almost all cases of reported altered specificity of Qβ replicase, a careful product analysis is lacking. Results from our laboratory [C. K. Biebricher and R. Luce, unpublished experiments; cf. also Vourmakis et al. (1976)] indicate that incorporation of nucleotides using inefficient templates may be due to de novo synthesis of RNA (Sumper & Luce, 1975) rather than to instruction by the inefficient template.

On the other hand, there are a number of templates, called *self-replicating*, that can indeed be amplified to high concentrations. Spiegelman and co-workers (Mills et al., 1967; Levisohn & Spiegelman, 1968, 1969) derived self-replicating RNA templates from Qβ RNA itself by inducing selection pressure. The resulting "variant" RNA species did not need host factor for replication and were replicated considerably faster than Qβ RNA itself. Other efficient templates are the 6S RNA found in vivo late in the Qβ infection process (Banerjee et al., 1969) and the so-called mini-, midi-, micro-, and nanovariant RNA species (Kacian et al., 1972; Mills et al., 1973, 1975; Schaffner et al., 1977) that are produced in template-free systems containing Qβ replicase. This type of RNA has been shown to result from de novo synthesis (Sumper & Luce, 1975; Biebricher et al., 1981a,b). Their chain lengths range from 80 to 250 bases; their replication rates are high. These properties make them ideal templates to investigate the reaction kinetics of replication. In the present work, we considered replication of these RNAs rather than that of Qβ itself as our model system. This allowed us to avoid the complications of describing multiple replication points and accounting for the large difference in template efficiency of the Qβ plus and minus strands, since these RNAs synthesize roughly equal amounts of both complementary strands.

The template can thus not be considered as a mere substrate of the replicase. Much of the information for replication resides in the template (Biebricher & Orgel, 1973). It has been shown that not only the primary sequence (Küppers & Sumper, 1975; Schaffner et al., 1977) but also the secondary and tertiary structures of the single-stranded RNA template (Mills et al., 1977; Biebricher et al., 1982) play decisive roles in the replication process. The real catalyst is thus the template–replicase complex in which replicase and template share equivalent catalytic roles. The kinetic behavior is complicated because one of the components of the active enzyme, the RNA, is also the replication product, while the replicase concentration (in vitro) is set by the experimental conditions. Two fundamentally different replication phases are thus observed (Biebricher et al., 1981b): an exponential phase where enzyme is in excess and the RNA concentration grows exponentially (Haruna & Spiegelman, 1965c; Pace & Spiegelman, 1966; Levisohn & Spiegelman, 1968) and a linear phase where RNA is in excess and is further synthesized at a nearly constant rate. Some of the complications of the in vitro experiments were not included in the kinetic model: the two complementary template species are not only amplified cross-catalytically but may also react with each other to form a double strand that is inactive as template; metastable RNA structures may be formed (Biebricher et al., 1982); the RNA does not have a unique sequence but is in reality a quasi-species distribution (Eigen, 1971; Eigen & Schuster, 1977) of related sequences.

Reaction Mechanism

Initiation. The first step of replication is complex formation between template and replicase. Qβ replicase binds rapidly to all single-stranded RNAs and even to double-stranded RNAs; the complexes with efficiently replicated RNA are more stable (August et al., 1968; C. K. Biebricher and R. Luce, unpublished experiments). Binding occurs preferentially at interior sites (Weissmann et al., 1973; Mills et al., 1977; Meyer et al., 1981). The connection between these binding sites and the binding that leads to initiation of replication (Weissmann, 1974) is not known. Furthermore, it cannot be excluded that additional steps, such as transport of the enzyme on the template to the 3′ end or conformation changes of the template, also take place. In the kinetic model, we have combined all these possible steps into a single binding step (Figure 1).

Initiation also requires geminal association of two (at least) GTP molecules at the 3′-terminal C cluster of the template. The rate of this geminal association is dramatically dependent

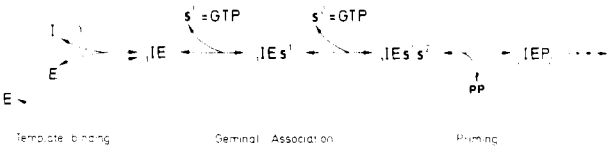

FIGURE 1: Initiation of replication: template binding, geminal association, and priming. Symbols as in Figure 4 and Table I. Instead of template binding from the constituents, the active template–enzyme complex $_1$IE may also be formed by rearrangement or by reaction of the inactive complex $_n$IE, in the latter case probably by binding new enzyme to the free 3′ end of the RNA followed by release of the old enzyme from the 5′ end (dotted lines).

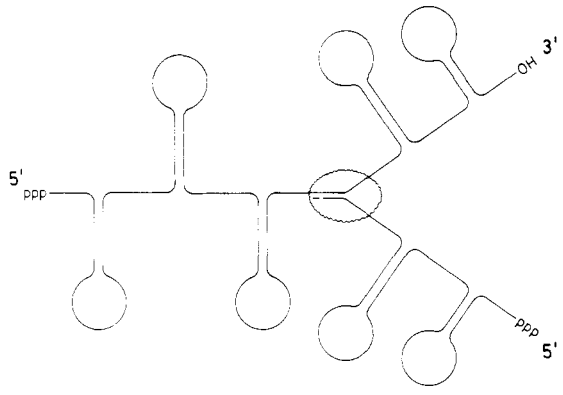

FIGURE 2: Elongation mechanism, adapted from models of Weissmann (1974) and Mills et al. (1978). At the replication fork, new substrate is added by base pairing with the template and pyrophosphate release. The short double helix at the replication fork is opened by the enzyme as replication continues.

on the structure of the template. It can be inhibited specifically by polyethylene sulfonate without affecting the template–replicase binding (Kondo & Weissmann, 1972a). While the geminal association rate does not determine the rate of replication when efficient self-replicating variants are used (Biebricher et al., 1981b), it does apparently determine the rate of replication of synthetic nucleotide copolymers (Blumenthal, 1980). Furthermore, at unphysiologically high GTP concentrations, Qβ replicase can be induced to accept inefficient templates, which indicates that the specificity of Qβ replicase is in part due to the rate of geminal association (Blumenthal, 1980). This is also supported by the finding that oligonucleotide primers circumvent the normal initiation process (Feix & Hake, 1975) and thus avoid discrimination by the geminal association rate. Formation of the first phosphodiester bond ("priming") is essentially irreversible under the conditions used in in vitro experiments, as it is under physiological conditions also. Since oligonucleotides are not found among the reaction products, priming must be considered to trap the enzyme on the template for the complete replication cycle.

Elongation. The elongation reaction consists of consecutive complexation and phosphodiester bond formation steps. The replication fork moves from the 3′ end of the template toward the 5′ end. Nevertheless, the role of the template is not merely instructing the nucleotide sequence of the replica. Since both replica and template must be single-stranded to be reusable as templates, they have to be separated from each other not far from the replication fork by some mechanism involving the enzyme (Weissmann et al., 1968; Weissmann, 1974). Furthermore, protection against spontaneous annealing of the single-stranded RNA must be insured by an energy barrier provided by strong intramolecular structuring (Figure 2; Mills et al., 1977, 1978; Biebricher et al., 1982). It is thus not surprising that structural characteristics of template and replica

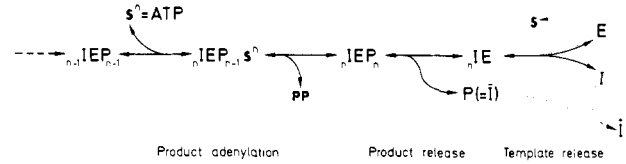

FIGURE 3: Termination of replication. Symbols as in Figure 4 and Table I. Elongation of the product strand is finished by adenylation, i.e., by incorporation of an adenylate residue at the 3′ end of the replica without base pairing to the template. Product release and template release free the two complementary strands from the enzyme. Additional interaction with substrate may be required to effect template release (dotted circle). Plus and minus strands may eventually anneal to form a double-strand $I^+ \cdot I^-$ inactive as template.

are reflected in dramatic position to position variations of the elongation rates: Some elongation steps proceed orders of magnitude more slowly than others (Rozovskaya et al., 1981; Aivazashvili et al., 1981) and can thus be seen as "pause sites" (Mills et al., 1978). Since these structural changes of the RNAs are not understood at the molecular level, they were not included explicitly in our kinetic model. In order to test the kinetic significance of such pause sites in the computer simulations, we reduced the rates of elongation at particular sites by changing the values of the rate constants for phosphodiester bond formation.

Termination. After completion of one replication round, the enzyme has reached the 5′ end of the template and the 3′ end of the replica. For non-self-replicating templates, the enzyme action is finished with completion of the template–replica double strand. Replication of self-replicating RNAs, however, requires recycling of template, replica, and enzyme (Figure 3). It has been shown that uninstructed adenylation (Rensing & August, 1969; Weber & Weissmann, 1970) and replica release are the first steps (Dobkin et al., 1979). Kinetic profiles of replication show pronounced slowing of replication rates at higher RNA concentrations (Kondo & Weissmann, 1972b), which is attributable to product inhibition. We thus assume replica release to be a reversible reaction, the reverse reaction being product inhibition. There is experimental evidence that the inactive template–enzyme complex has to dissociate (Dobkin et al., 1979) in order to reactivate enzyme and template. The dissociation step is slow and often rate determining (Biebricher et al., 1981b). It is possible that a conformational change of the enzyme is required for reactivation [cf. Landers et al. (1974)], perhaps effected by nucleoside triphosphates.

Replication. Compilation of the experimental evidence thus leads to the reaction scheme shown in Figure 4 as the minimal scheme that is able to describe RNA replication by Qβ replicase.

Analytical Theory

For an RNA with n monomers, the mechanism shown in Figure 4 has $4n + 2$ intermediates and $10n + 28$ mostly nonlinear rate terms. While computer simulations of the full mechanism (see Computer Simulations) are feasible, gaining insight into it by analytical approaches requires appropriate simplifications and approximations. In a subsequent paper, these simplifications will be relaxed, in particular in order to express the effects of competition between plus and minus strand replication kinetics.

We assumed the following: (1) Reactions resulting in loss of template RNA are absent; the RNA and template concentrations are thus always equal. (2) Corresponding rates in the plus and the minus strand cycles are equal (see Discussion). Plus and minus strands are then kinetically indis-

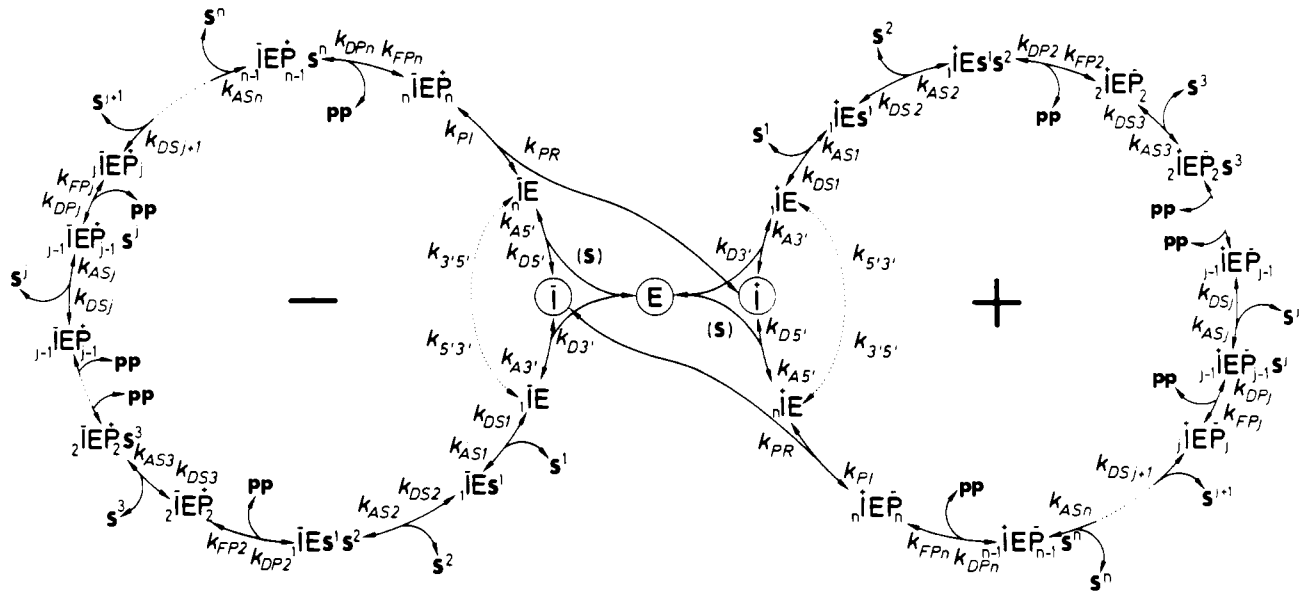

FIGURE 4: Complete replication mechanism, combining the initiation, elongation, and termination steps of both cross-catalytic cycles (cf. Figures 1–3). The indices + and − of the rate constants for the two cycles have been omitted for clarity, but corresponding steps of the two cycles may have different rates. The species and rate constant symbols are explained in Table I.

tinguishable. This is of course always the case when the RNA has a palindromic sequence. The double cycle depicted in Figure 4 then coalesces into a single cycle (Figure 5), and the cross-catalytic process in Figure 4 becomes autocatalytic amplification of template. (3) Competition between different RNA species does not occur. The limited accuracy of replication resulting in a quasi-species distribution (Eigen & Schuster, 1977) is thus disregarded. (4) No specific sequence was attributed to the RNA. Each position (j) of the RNA was considered to be occupied by a defined but not specified nucleotide S^j even though the 5′- and the 3′-terminal sequences are invariably $_{ppp}$G-G-G- or -C-C-C-A_{OH}, respectively. The concentrations of the four substrates ATP, CTP, GTP, and UTP were expressed explicitly in deriving the equations; so that the analogy to Michealis–Menten formulas could be stressed, an effective substrate concentration ($[S_0]$), given by the weighted harmonic mean

$$1/[S_0] = f_A/[ATP] + f_C/[CTP] + f_G/[GTP] + f_U/[UTP]$$

where the f values are the fractions of each nucleotide in the RNA, was introduced. (See Table I for symbols.)

(1) Linear Growth Phase. The steady-state approximation usually made in enzyme kinetics to derive Michaelis–Menten expressions must be used with caution, as the active catalyst has two components, one of which—the RNA template—is also a product of the reaction.

For total RNA concentrations large compared to the total enzyme concentration ($[E_0]$), the complex concentrations ($[_jIEP_j]$) are constant, the free and total RNA concentrations ($[I]$ and $[I_0]$, respectively) grow linearly, and the steady-state approximation can be applied. During this growth phase, $[I] = [I_0] - [E_0] - [_nIEP_n]$; the latter term is only of consequence when product inhibition becomes important. The equations one derives for the RNA production rate v in the palindromic cycle (Table II) by setting the time derivatives of all intermediate concentrations to zero have forms analogous to ordinary Michaelis–Menten formulas, with the turnover number k_T, Michaelis constant K_M, and inhibition parameter K_H being given by complicated functions of the elementary reaction rate constants (Figure 5). A growth rate independent of enzyme concentration is obtained by defining $\kappa = v/[E_0]$. The steady-state approximation can be seen from the detailed equations given in Figure 5 to be equivalent to finding an inverse first-order rate constant by summing the residence times at each stage over a complete replication round assuming that the phosphodiester formation step is irreversible. The fact that a conventional Michaelis–Menten form is obtained means that its parameters v_{max}, K_M, and K_H can be obtained by the usual procedures of enzyme kinetics, e.g., by Lineweaver–Burk plots of $1/v$ vs. $1/[S_0]$ at various values of $[I_0]$.

It is at present uncertain whether nucleoside triphosphates participate in the replication process other than as components for the growing replica chain. Since nucleoside monophosphates are not found among the reaction products, triphosphates apparently do not function as energy sources by hydrolysis. If they do act without hydrolysis as effectors of chain transport, then the k_{FPj} terms as given can be understood to account formally for this action also. If they are required to effect replica or template release, then additional substrate dependence (Table II) appears in the k_{PR} and $k_{DS'}$ terms. The values of k_T and K_M are affected; since template and replica are tightly bound to the enzyme, their release rates can be rate limiting for the replication process.

The expressions in Table II and Figure 5 show several characteristic features of the reaction mechanism: (1) The total enzyme concentration $[E_0]$ enters throughout the rate expressions in first order, as confirmed experimentally for template-instructed replication but not for de novo synthesis of RNA (Biebricher et al., 1981b). (2) A transition from linear dependence upon substrate concentration to saturation occurs for $[S_0]$ in the range of K_M. The ansatz relating $[S_0]$ to individual nucleoside triphosphate concentrations expresses starvation and saturation effects if individual concentrations take on extreme values. If at very low substrate concentrations—in particular at low $[S^1]$ and $[S^2]$—initiation becomes rate limiting, then a stronger than linear dependence upon substrate concentration prevails. (3) Each elongation step appears individually in the Table II expressions. The irregular nature of the elongation rate caused by "pause sites" is not hidden by averaging over rate parameters.

While for very long chains such as Qβ itself the elongation process would be rate limiting, for short chains other steps such as template reactivation may be slower. Two alternatives have

Table I

Mathematical Symbols	
n	length of nucleotide chain
j	index denoting stage of elongation
λ	eigenvalues
$\mathbf{K}$	matrix of rate constants
$\mathbf{E}$	unit matrix
Species Symbols	
I	free template (information carrier)
P_n	replica = new template
E	free enzyme
$_1IE$	active enzyme–template complex
S^j	substrate at position j of replica
$_1IES^1$	first replication complex
$_1IES^1S^2$	geminal association complex
$_jIEP_j$	chain elongation complex (also I_j)
$_jIEP_jS^{j+1}$	substrate recognition complex ($2 \leq j \leq n-1$)
$_nIE$	inactive enzyme–template complex
Concentrations	
$[I_0]$	total template concentration
$[E_0]$	total enzyme concentration
$[E_0^+]$	total enzyme concentration associated with plus strand
$[E_0^-]$	total enzyme concentration associated with minus strand
$[S_0]$	effective substrate concentration
Elementary Reaction Rate Constants[a]	
k_{ASj}	association of substrate S^j
k_{AS}	average association of substrate (1×10^8)
k_{DSj}	dissociation of substrate S^j (1×10^5 for $j = 1$)
k_{DS}	average dissociation of substrate S (2×10^4 for $j \neq 1$)
k_{FPj}	formation of phosphodiester linkage by incorporation of substrate S^j into replica (1 for $j = 2$)
k_{FP}	average phosphodiester linkage formation (5 for $j > 2$)
k_{DPj}	pyrophosphorolysis at position j
k_{DP}	average pyrophosphorolysis (2×10^3)
k_{PR}	product release (0.5)
k_{PI}	product inhibition (2.5×10^5)
$k_{5'3'}$	direct reactivation of enzyme–template complex (0)
$k_{3'5'}$	reverse direct reactivation (0)
$k_{D5'}$	dissociation of enzyme from inactive position on template (1×10^{-2})
$k_{D3'}$	dissociation of enzyme from active position (1×10^{-5})
$k_{A5'}$	association of enzyme at inactive position of template (1×10^7, 1×10^5)
$k_{A3'}$	association of enzyme at active position of template (1×10^7)
Composite Rate Parameters	
k^*_{12}	initiation rate parameter
k^*_{PR}	product release
k^*_{TR}	template release and enzyme reactivation
k^*_{TB}	template binding
k^*_{T1}	substrate turnover and product release
k^*_{T2}	5′3′ reactivation
$k^*_{A5'}$	$k_{A5'}[E_0]$
k^*_{S1}	binding of first substrate
k^*_{S2}	binding of second substrate
k^*_{SB}	successive substrate binding and incorporation
κ	growth rate
κ_1	overall rate of replica synthesis
κ_j	substrate incorporation rate constant
κ_n	net reactivation rate constant
Other Parameters	
v	steady-state RNA production rate
v_{max}	saturation steady-state RNA production rate
k_T	turnover number
k_c	competition rate constant
K_M	Michaelis constant
K_S	average substrate association constant
$K_{S'}$	average substrate association constant, including substrate-mediated reactivation
$K_{3'5'}$	coupling to reactivation
K_H	inhibition constant
$K_{\Sigma IE}$	overall template–enzyme interaction constant

[a] Standard values for the simulations are in parentheses. Units are moles per liter and seconds.

to be considered for template reactivation: dissociation of the 5′-bound template followed by reassociation at the 3′ end and intramolecular transport of the template from 5′ to 3′ binding. The two alternatives are kinetically indistinguishable unless the concentrations of plus and minus strands are measured separately.

Table II: Summary of Equations Describing Linear Growth Phase

reaction velocity	$v = \dfrac{k_T[E_0][S_0]}{K_M + [S_0]\{1 + K_H[I]\}}$
turnover number (k_T)	$\dfrac{1}{k_T} = \underbrace{\sum_{j=2}^{n} \dfrac{1}{k_{FP_j}} + \dfrac{1}{k_{PR}} + \dfrac{1}{k_{D5'}}}_{k^*_{T1}} \underbrace{\left(1 + \dfrac{k_{A5'}}{k_{A3'}}\right) + \dfrac{1}{k_{A3'}[I]}}_{k^*_{T2}}$ substrate turnover and product release; 5′3′ reactivation
Michaelis constant (K_M)	$K_M = k_T\left[\dfrac{1 + K_{3'5'}}{k^*_{12}} + \dfrac{1}{k^*_{SB}}\right]$
chain initiation	$\dfrac{1}{k^*_{12}} = \dfrac{[S_0]}{k_{AS1}[S^1]}\left\{1 + \dfrac{(k_{FP2} + k_{DS2})k_{DS1}}{k_{FP2}k_{AS2}[S^2]}\right\}$
coupling parameter for reactivation	$K_{3'5'} = \dfrac{k_{D3'}k_{A5'}}{k_{A3'}k_{D5'}} + \dfrac{k_{D3'}}{k_{A3'}[I]}$
successive substrate binding	$\dfrac{1}{k^*_{SB}} = \sum_{j=2}^{n} \dfrac{k_{FP_j} + k_{DSj}}{k_{FPj}} \dfrac{[S_0]}{k_{ASj}[S^j]}$
inhibition parameter (K_H)	$K_H = \dfrac{k_{PI}}{k_{PR}} \dfrac{k_T}{k_{D5'}}\left\{1 + \dfrac{k_{A5'}}{k_{A3'}}\left(1 + \dfrac{k_{D3'}}{k^*_{12}[S_0]}\right)\right\}$
free template concentration	$[I] = [I_0] - [E_0] - [_nIEP_n]$

If direct 5′3′ reactivation occurs in parallel with the dissociative mechanism, the following expressions replace the ones given above:

$$K_{3'5'} = \frac{k_{3'5'}}{k_{5'3'}} + \frac{k_{D3'}k_{5'3'} + k_{D5'}(k^*_{12} + k_{3'5'} + k_{D3'})}{[k_{5'3'}(k_{A3'} + k_{A5'}) + k_{D5'}k_{A3'}][I]}$$

$$K_H = \frac{k_{PI}}{k_{PR}} \frac{k_T}{k_{5'3'}}\left(1 + \frac{k_{3'5'}}{k^*_{12}}\right)$$

k^*_{T2} = above expression for $k^*_{T2} + 1/k_{5'3'}$

Physical insights can be gained by deriving simplified rate expressions for special limiting cases. For this purpose, let us assume that no specific, substrate-dependent elementary step is rate determining, that the RNA concentration is not so high that inhibition is important, i.e., $K_H[I_0] \ll 1$, and that phosphodiester bond formation is slower than substrate dissociation, i.e., $k_{FPj} \ll k_{DSj}$. An average substrate association constant $K_S = k_{DS}/k_{AS}$ independent of chain position can be introduced, where k_A and k_D are the average substrate association and dissociation rate constants, whereupon the sum terms in k^*_{12} and k^*_{SB} (and possibly k_T, cf. case 4 below) simplify to $K_S/(k_{FPj}[S_0])$.

Case 1. Assume that the chain length n is large, so that elongation is rate limiting. The sum terms then dominate all the others. Let k_{FP} represent an average k_{FPj}. Then the Table II expressions simplify to

$$k_T = k_{FP}/n$$

$$K_M = K_S = k_{DS}/k_{AS}$$

$$v = \frac{k_{FP}[E_0][S_0]/n}{[S_0] + K_S}$$

Case 2. Assume that the substrate concentration is lowered until initiation becomes rate limiting, i.e., until $k^*_{12} \ll k^*_{SB}$, and that reactivation is irreversible; then the rate becomes

$$v = \frac{k_{FP}[E_0][S_0]^2}{K_S^2}$$

Case 3. Assume that reactivation, i.e., dissociation of 5′-bound template and association of 3′-bound template, is rate limiting. Two kinetically distinguishable mechanisms are possible depending on whether substrate (e.g., GTP) binding is involved in reactivation. If it is not, then the rate is

$$v = \frac{k_{D5'}[E_0][S_0]}{[S_0] + nK_Sk_{D5'}/k_{FP}}$$

where reassociation has been neglected, such that $k_T = k_{D5'}$; $1/k^*_{12}$ has been neglected compared to $1/k^*_{SB}$, such that $K_M = k_T/k^*_{SB}$; and k^*_{SB} has been simplified to nK_S/K_{FP}.

Case 4. If reactivation is rate limiting and substrate binding is required, the rate is

$$v = \frac{k_{D5'}[E_0][S_0]}{[S_0] + K_S'}$$

in which a new Michaelis constant, K_S', appears, given by the fact that the expression $1/k^*_{SB}$ changes to $1/k^*_{SB} = K_S(1/k_{D5'} + n/k_{FP}) \simeq K_S/k_{D5'}$ while k_T remains unchanged.

It can be seen that cases 3 and 4 show a common turnover number but different Michaelis constants, while cases 1 and 4 have a common Michaelis constant but different turnover numbers. We will discuss later whether kinetic data allow distinctions to be made between these cases.

(2) *Exponential Growth Phase.* Saturation of enzyme with template in the linear growth situation permitted us to apply the steady-state approximation in a traditional, if complicated manner. We now turn to the growth kinetics where enzyme is so greatly in excess of template that it is the templates that are saturated with enzyme and where apart from an induction

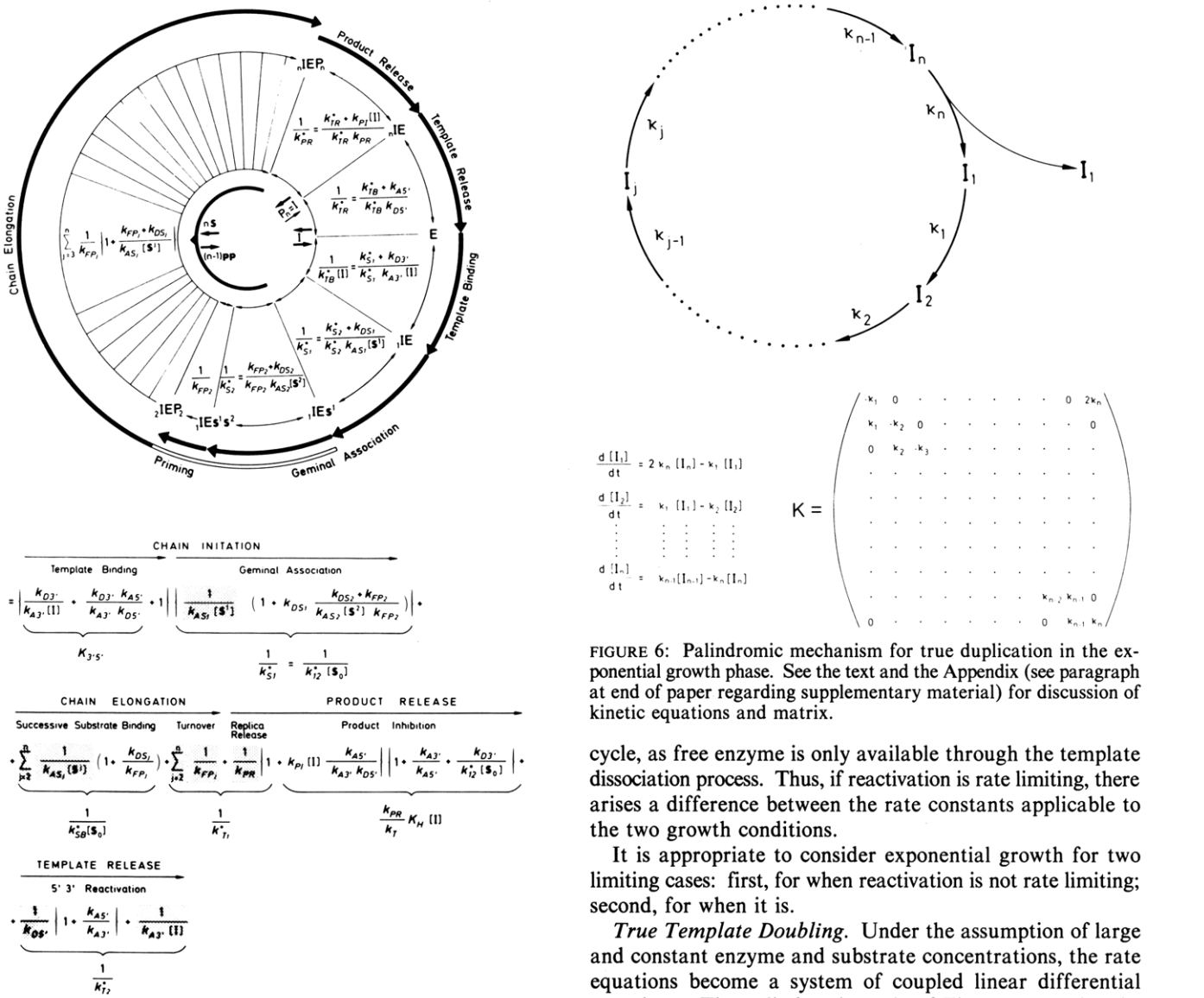

FIGURE 5: Condensed palindromic mechanism and steady-state rate constant expressions. The equations for template release are based on the assumption that substrate is not required for reactivation (see text). The growth constant κ in the linear growth phase is $v/[E_0]$. The shaded terms indicate contributions to residence times from successive forward reactions; the remaining terms arise from back-coupling. The free template concentration, [I], is close to $[I] = [I_0] - [E_0] - [_nIEP_n]$; the exact equation $[I] = [I_0] - [E_0] - [_nIEP_n] + [E]$ holds at all times.

period—to be discussed later—their total concentration follows first-order kinetics and grows exponentially:

$$d[I_0]/dt = \kappa[I_0]$$

$$[I_0] = [I_0]_{t=0}e^{\kappa t}$$

Exponential growth of the total template concentration, however, implies that the concentrations of all of the intermediates also grow exponentially, and so the ordinary steady-state approximation does not apply. After an initial transient period, the ratios of the intermediate concentrations remain constant during the exponential growth process. A further difference from the linear growth situation concerns the start of a new replication cycle. During exponential growth, one new cycle starts when the replica RNA leaves the replication complex and binds to a free enzyme molecule, another when the template RNA itself is reactivated either through dissociation and rebinding or through a direct pathway. In linear growth, only the second of these starts a new

FIGURE 6: Palindromic mechanism for true duplication in the exponential growth phase. See the text and the Appendix (see paragraph at end of paper regarding supplementary material) for discussion of kinetic equations and matrix.

cycle, as free enzyme is only available through the template dissociation process. Thus, if reactivation is rate limiting, there arises a difference between the rate constants applicable to the two growth conditions.

It is appropriate to consider exponential growth for two limiting cases: first, for when reactivation is not rate limiting; second, for when it is.

True Template Doubling. Under the assumption of large and constant enzyme and substrate concentrations, the rate equations become a system of coupled linear differential equations. The palindromic cycle of Figure 5 can then be simplified as shown in Figure 6. Here, each stage of the elongation process is identified by a subscript denoting the degree of replica polymerization attained, I_1 representing both free RNA and the replication complex before formation of the first phosphodiester bond. The rate constants for the $n - 1$ polymerization steps are

$$\kappa_j = k_{FPj}\frac{[S_0]}{K_S + [S_0]}$$

while κ_n is the effective rate constant for the overall reactivation process. The system of rate equations for all (n) compounds I_j is characterized by a matrix **K** of rate coefficients shown in Figure 6. The rate equations (Figure 6) are solved by finding the eigenvalues of the determinental equation

$$\det(\mathbf{K} - \lambda\mathbf{E}) = 0$$

where **E** is the unit matrix. This equation has the polynomial form

$$\prod_{j=1}^{n}(\kappa_j + \lambda) = 2\prod_{j=1}^{n}\kappa_j$$

Sign rules applied to this polynomial suggest that it has only one positive real root and that the corresponding eigenvalue is the exponential growth constant for all compounds I_j (which is not, however, the same as the linear growth constant $\kappa[E_0]$; see below).

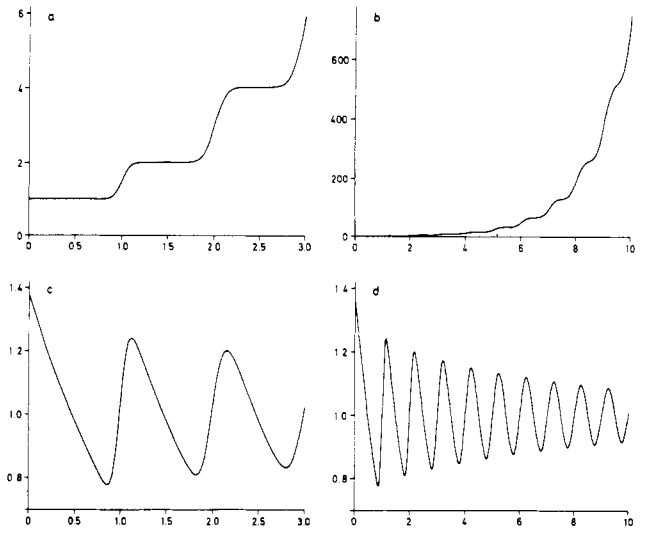

FIGURE A3: (a and b) Time dependence of the total concentration of free and complexed complete templates for $n = 200$, from eq 26 of the Appendix. (See paragraph at end of paper regarding supplementary material.) (c and d) Ratio of eq 26 to its first term, giving the oscillatory modulation factor of the growth function. Ordinates are in units of the initial concentration $x_1(0) = C_0$ and abscissas in units of n/k. The modulation factors decay to 1 at long times as coherent exponential growth is established. They differ from 1 at $t = 0$ because the initial induction phase, where the modulations are at first unsymmetric and then sinusoidal, delays onset of exponential growth.

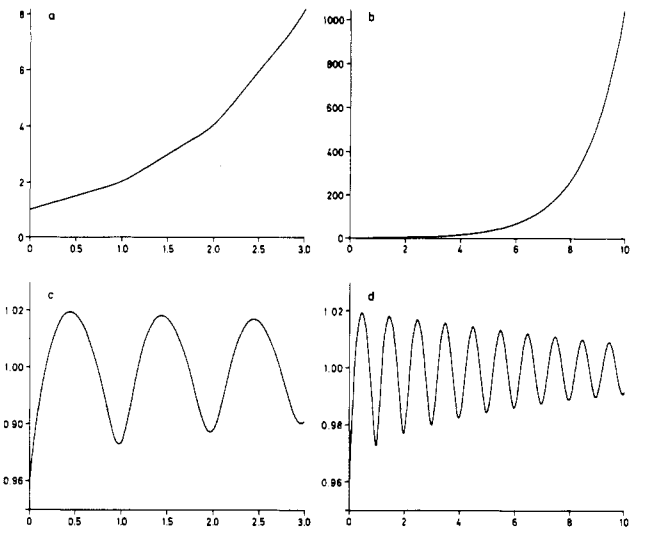

FIGURE A4: (a and b) Time dependence of the total amount of polymer, scaled to the complete chain length $n = 200$, from eq 27 of the Appendix. (See paragraph at end of paper regarding supplementary material.) (c and d) Equation 27 divided by its first term. Coordinates as in Figure A3. The steplike behavior of the complete template profiles (Figure A3a,b) is replaced by smoother total polymer profiles, showing more closely exponential growth and smaller modulation factors.

The nature of the growth constant can be understood by analyzing the solution for the simple case of all κ_j (including κ_n) being equal. Then the characteristic equation is

$$(\kappa + \lambda)^n = 2\kappa^n$$

with n eigenvalues

$$\lambda_m = \kappa[2^{1/n} \exp(2\pi im/n) - 1]$$

where $\exp(2\pi im/n)$ is the mth root of unity (see Appendix in supplementary material for details). The real positive eigenvalue is

$$\lambda_n = \kappa(2^{1/n} - 1)$$

which for large n becomes (κ/n) ln 2. This is smaller by the factor ln 2 than the linear growth constant κ/n which pertains for the same assumptions made here; if a single step is rate limiting, the ln 2 factor disappears and the linear and exponential growth constants become identical. Under Computer Simulations, the factor is indeed shown to lie somewhere between ln 2 and 1 depending on the choice of rate constants.

The complete analytical solution describes in detail not only the exponential growth phase but also the induction period preceding it, which includes decaying oscillations. Since the induction period kinetics are of interest in themselves and propagate secondary effects well into the exponential growth phase, further explication is provided in the Appendix (see paragraph at end of paper regarding supplementary material). Figures A3 and A4 from the Appendix display the solutions for sums of concentrations at early times for $n = 200$. The total concentration of complete RNA chains, $\sum_{j=1}^{n} x_j(t)$, is seen to start at the initial concentration, c_0, and increase stepwise in a geometric progression, while the total amount of macromolecular RNA (normalized to the length of a complete chain) $1/n\sum_{j=1}^{n}(n + j)x_j(t)$, starts to increase linearly and increases its slope stepwise in a geometric progression. The steplike changes are thus superimposed upon the underlying exponential growth, which they finally modulate by a sinusoidal function with decreasing amplitude. An expansion of the expressions for large values of n shows that the oscillatory mode with $m = 1$ persists much longer than any of the modes with $m > 1$, the decay constants being proportional to $(m/n)^2$. Figures A3c,d and A4c,d show the sum functions divided by the growth terms. It is seen that the oscillatory modes superimposed upon the growth asymptotically reduce to sinusoidal forms represented by the longest persisting oscillatory mode.

For present purposes, it is important to recognize that both the complete analytical treatment of the simplified mechanism (Figure 6) and computer simulations of the detailed mechanism (Figure 4) confirm that for the rapid reactivation case all intermediate concentrations do grow coherently as suggested by the equations given in this section.

Slow Reactivation. While for the fast reactivation case there is a close relationship between linear and exponential growth kinetics, slow reactivation implies essential differences between them. Their causes can be explored by means of the skeleton mechanism shown in Figure 7, where the palindromic cycle is considered to have only two steps: reactivation, a reversible process proceeding through 5′ and 3′ association and dissociation, and everything else.

Consider the limiting case where extremely slow reactivation dominates the replication kinetics. If RNA is in excess, growth is blocked by the reactivation bottleneck, for new replication cycles can only start when enzyme is eventually set free by 5′ dissociation. If enzyme is in excess, however, one new replication cycle begins quickly upon product release even if the second is blocked at the reactivation bottleneck. Now relax the bottleneck somewhat to allow slow 5′ dissociation to proceed. While the linear growth rate (RNA excess) is accelerated only by the amount that the bottleneck itself has been widened, the exponential growth rate (enzyme excess) is multiplied by the doubling effect of rapid replica release.

This behavior is clearly expressed in the rate equations (Figure 7) describing the situation of enzyme excess. The solution to the linear differential equations has two eigenvalues, a negative one characterizing the approach to exponential growth and a positive one characterizing the rate of exponential growth itself. Two limiting cases are of special interest:

Case 1. Both $k_{D5'}$ and $k^*_{A5'}$ are small compared to κ_1. The exponential growth constant is the geometric mean of κ_1 and

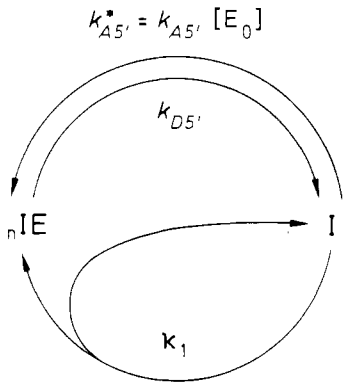

FIGURE 7: Simplified reaction mechanism for rate-limiting, reversible reactivation. The differential equations

$$d[_nIE]/dt = -k_{D5'}[_nIE] + (\kappa_1 + k^*_{A5'})[I]$$

$$d[I]/dt = k_{D5'}[_nIE] - k^*_{A5'}[I]$$

have the eigenvalues

$$\lambda = \frac{k_{D5'} + k^*_{A5'}}{2}\left\{-1 \pm \left[1 + \frac{4\kappa_1 k_{D5'}}{(k_{D5'} + k^*_{A5'})^2}\right]^{1/2}\right\}$$

which simplify to

$$\lambda = \pm(\kappa_1 k_{D5'})^{1/2} \text{ for } \frac{4\kappa_1 k_{D5'}}{(k_{D5'} + k^*_{A5'})^2} \gg 1$$

and

$$\lambda = \frac{\kappa_1 k_{D5'}}{k_{D5'} + k^*_{A5'}} \text{ and } -(k_{D5'} + k^*_{A5'}) \text{ for } \frac{4\kappa_1 k_{D5'}}{(k_{D5'} + k^*_{A5'})^2} \ll 1$$

$k_{D5'}$, the replication and reactivation rate constants. Since κ_1 is assumed here to be greater than $k_{D5'}$, the exponential growth constant is greater than the linear one.

Case 2. The sum $k_{D5'} + k^*_{A5'}$ is greater than the geometric mean of κ_1 and $k_{D5'}$. Since for slow reactivation κ_1 is assumed to be large compared to $k_{D5'}$, this can occur only when $k^*_{A5'}$ is comparable to or larger than κ_1. The positive eigenvalue is then $\kappa_1 k_{D5'}/k^*_{A5'}$. The turnover number expression in Table II shows that for slow reactivation the growth constant in the linear phase is $k_{D5'}/(1 + k_{A5'}/k_{A3'})$, which translated to the skeleton mechanism of Figure 7 becomes $k_{D5'}/(1 + k^*_{A5'}/\kappa_1)$. Again the growth rate is greater in the exponential growth phase than in the linear growth phase.

(*3*) *Transition from Exponential to Linear Growth.* When the RNA concentration becomes comparable to the free enzyme concentration, the latter is no longer constant. The equations derived by linearizing the growth equations are no longer valid—the growth rate falls more and more below that of the exponential phase and approaches the linear growth rate. Finally there is enough RNA to saturate the enzyme completely, and the steady-state equations for the linear phase can be applied. An analytical description of the nonlinear kinetic behavior in the transition range would require drastic simplifications, which we do not think would bring useful insights. Two important points, however, do need to be addressed: Is there a sharp transition from exponential to linear growth, and, if so, at which concentration ratio of $[I_0]$ to $[E_0]$ does it occur?

The analogy of the approach to saturation to a titration of the enzyme with RNA, based on the interaction between RNA and enzyme, is obvious. We define an approximate interaction constant $K_{\Sigma IE}$

$$K_{\Sigma IE} = \frac{[\Sigma IE]}{[I][E]} = \frac{[\Sigma IE]}{([I_0] - [\Sigma IE])([E_0] - [\Sigma IE])}$$

and can solve the expression for $[\Sigma IE]$, which comprises all steady-state (rather than equilibrium) concentrations of the enzyme–template intermediates, to get equations well-known in titration theory (Winkler-Oswatitsch & Eigen, 1979). Strictly speaking, the above expression would refer only to the linear growth phase where steady-state concentrations are clearly defined. For very strong enzyme–template interactions, $K_{\Sigma IE}^{-1} \ll [E_0] + [I_0]$ and sharp end-point behavior appears, i.e., $[\Sigma IE] = \inf([E_0],[I_0])$ where inf (=infimum) means the smaller of the two concentrations $[E_0]$ and $[I_0]$. For weak enzyme–template interaction, we would expect a smooth transition between exponential and linear growth starting well before equimolarity of enzyme and RNA.

For large values of $K_{\Sigma IE}$, the onset of linear growth should be quite sharp and occur at $[I_0]$ values between $[E_0]$ and $2[E_0]$. Once all enzyme is saturated with template—as is the case when replication is started with equimolar template and enzyme—each active complex can produce one replica before enzyme reactivation becomes a prerequisite for further reaction (Biebricher et al., 1982). For RNA growth starting from $[I_0] \ll [E_0]$, the transition from exponential to linear growth should start at $[I_0] = [E_0]$ and be completed at $[I_0] = 2[E_0]$. Experimental investigation of the transition range supplied evidence for this case (Biebricher et al., 1981b).

In the above considerations, we have assumed, as throughout this paper, that a template cannot engage simultaneously more than one enzyme molecule. That assumption is not true for long template chains (Weissmann, 1974). For RNA able to bind up to m enzyme molecules per template strand, a continuous transition would be expected to extend from $[I_0] = [E_0]/m$ with $1 < m < \bar{m}$, where $\bar{m}$ is the maximum number of enzymes per template strand (occupancy), and $[I_0] = 2[E_0]$, accompanied by a continuous decline of occupancy. It is important that multiple occupancy does not occur for short templates, as it would also result in a large difference of growth rates in the exponential and the linear growth range.

(*4*) *Conclusions of Analytical Theory.* The results obtained by analytical investigation of the reaction mechanism and their implications for interpretations of rate measurements are summarized in Table III.

Computer Simulations

The reaction mechanism assumed for computer modeling is the set of elementary reactions corresponding to the scheme shown in Figure 4. It is somewhat expanded from that discussed in an earlier paper (Biebricher et al., 1981b) to take into account the direct reactivation pathway (Dobkin et al., 1979). The standard set of rate constants shown in Table I was produced by intuition based upon general experience with the rates and stability constants of complex formation reactions, augmented by guesses as to the rate constants of phosphodiester bond formation. The stability constant for the 5′-bound enzyme–template complex was chosen so that the rate constant for dissociation, $k_{D5'}$, would give general agreement with the replication rates observed in in vitro replication experiments. The rate constant for product inhibition, k_{PI}, was varied so as to find the RNA concentration range where inhibition would appear as it was found in the laboratory. Otherwise, no attempts were made to adjust rate constants so as to bring the model into closer agreement with observations.

The number of differential equations to be integrated is large, $4n + 7$, and the range of reaction rates is wide. This combination implies that for large n one must use sophisticated integration algorithms in order to achieve acceptable integration times. Some of the computations were done on a CYBER 170 computer using the LSODE coding of Gear's al-

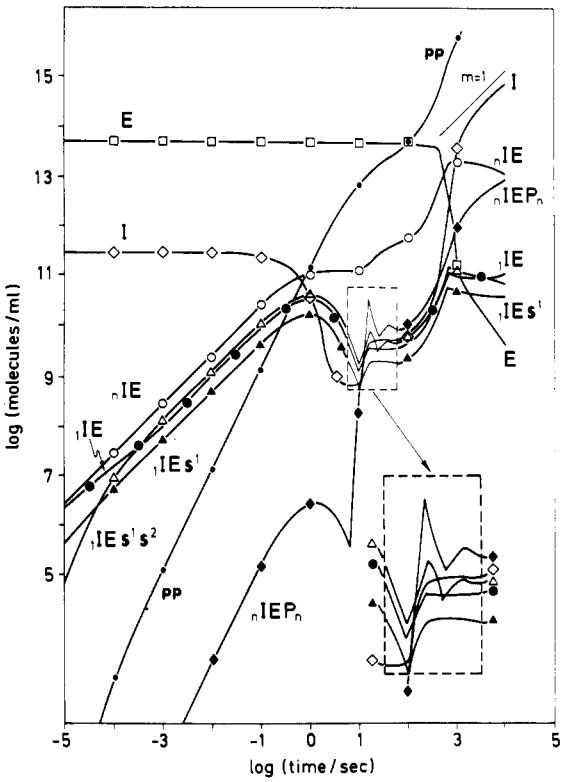

FIGURE 8: Profiles for $n = 50$ and the standard set of rate constants for the starting conditions $[I^+] = [I^-] = 10^{-10}$ M, $[E] = 10^{-7}$ M, and $[S_0] = 5 \times 10^{-4}$ M; all other concentrations are zero. Symbols as in Figure 4. Linear growth of [I] would have slope $m = 1$ as shown by the fine line.

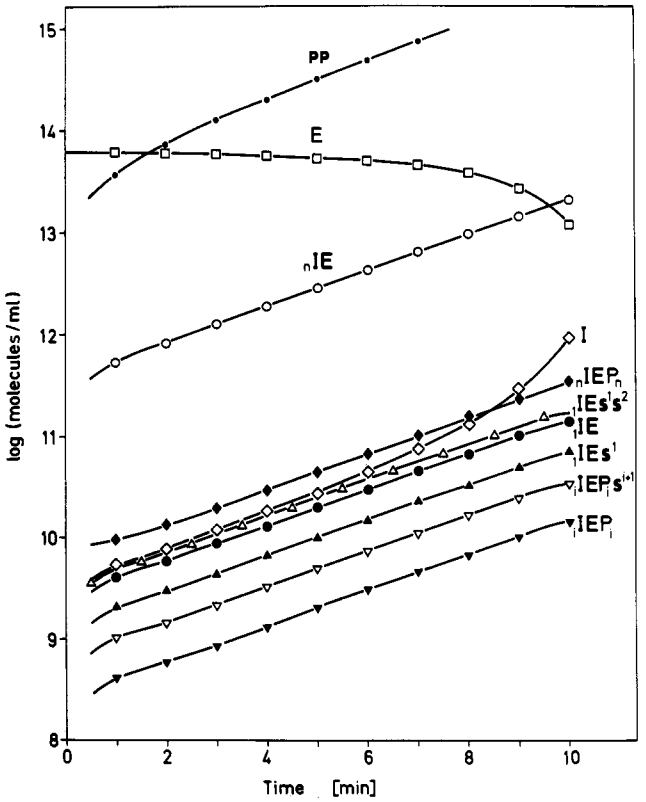

FIGURE 9: Semilogarithmic presentation of profiles for the exponential growth phase. Conditions and rate constants as in Figure 8.

gorithm (Hindmarsh, 1980). The remainder were done on a Univac 1100/82 computer using the selected asymptotic integration method of Young & Boris (1977). In the latter case, it was necessary to reduce the stiffness of the system of differential equations by taking the rate constants for the fastest complex formation reactions to be 100 times smaller than those shown in Table I in order to achieve the level of accuracy (10^{-3} relative accuracy for each species at all times) that was maintained in the CYBER computations. It was confirmed by repeating some of the Univac computations on the CYBER that none of the conclusions discussed here were affected by this change; the Young and Boris algorithm is, however, not accurate enough to maintain mass conservation for this mechanism at long reaction times.

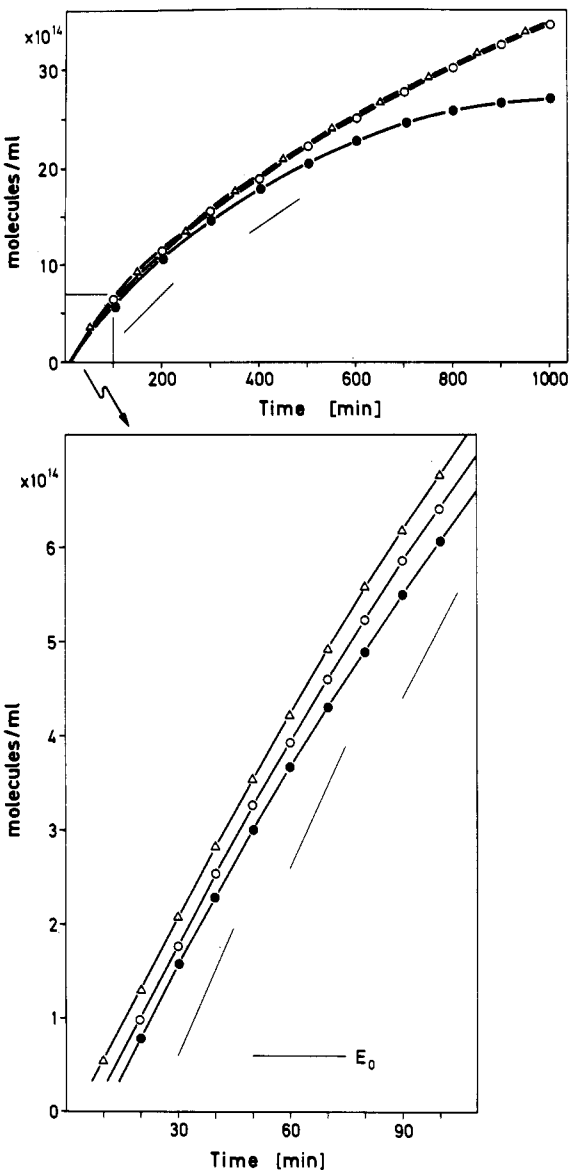

FIGURE 10: Free and total concentrations in the linear growth phase. (●) I^+ concentration for conditions as in Figure 8; (○) $[I^+]$ and (△) $[I_0^+]$ for conditions as in Figure 8 except $n = 10$. Fine lines indicate slopes calculated from Table II equations. The leveling off of the $[I^+]$ profile for $n = 50$ at long times is due to depletion of substrate.

We consider first the overall dynamics of the system of differential equations for a chain length of 50 nucleotides and for the initial conditions of 10^{-7} M enzyme concentration (equivalent to 200 molecules per *Escherichia coli* cell), 5×10^{-10} M concentration of I^+ and I^- RNA strands (1 of each per *E. coli* cell), 5×10^{-4} M nucleoside triphosphate concentration (a typical starting concentration for laboratory in vitro experiments), and all other initial concentrations zero. Computed profiles for the key species are shown in Figure 8 in log–log presentation from 10^{-5} to 10^4 s, in Figure 9 in semilog presentation from 0 to 10 min, the exponential phase

Table III: Interpretation of Experimental Results

experiment	data reduction	interpretation
(1) measure total RNA production rate for a range of $[E_0]$ and $[I_0]$ values	define concentration ranges for exponential growth, linear growth, and saturation	correct rates in linear range by K_H term; compute κ in exponential and linear growth phases
(2) investigate dependence of κ on $[S_0]$ in exponential and linear growth phases	determine v_{max} and K_M for both growth phases	(a) equal K_M and κ values for both phases imply reactivation not rate limiting (b) κ notably larger in exponential phase implies reactivation is rate limiting; if K_M is then equal in both phases, nucleoside triphosphate binding is also required for reactivation
(3) investigate $[S_0]$ dependence of κ at very low $[S_0]$ values	test for linearity	a stronger than linear dependence implies initiation is rate limiting
(4) measure relative amounts of plus and minus strands produced	test for balanced RNA production rates in complementary strands	if rates are balanced, above interpretations are valid; otherwise, more complicated expressions pertain
(5) make careful rate measurements for transition between exponential and linear growth	compare $[I_0]$ and $[E_0]$ at transition point	sharpness of transition is measure of enzyme–template binding strength; ratio $[I_0]/[E_0]$ must be between 1 and 2 at transition to exclude multiple replication points
(6) study details of mechanism by substrate starvation and separation of intermediates	assign rate-limiting effects to specific steps; calculate rates from intermediate concentrations	development of more detailed kinetic models

for these conditions, and in Figure 10 in linear presentations from 0 to 100 and 1000 min. The following characteristic features appear: (1) The concentrations of the intermediate complexes rise linearly or quadratically with time for the first 100 ms, depending on whether the intermediate is formed directly from the starting materials or requires prior formation of some other intermediate(s). (2) Depletion of RNA starting material begins to be noticeable at about 100 ms, and all profiles adjust themselves to quasi-stationary values over the first minute of reaction. During this time, there are some very sharp changes as material which entered the replication process at earlier times runs into the slow steps at the end of the elongation process. The oscillations that appear are real implications of the differential equations, not artifacts of the numerical integration algorithms. (3) From about 1-min to about 10-min reaction time, a phase of exponential growth occurs for all concentrations except for free RNA, which begins to accumulate more rapidly than the other species after about 5 min. The exponential growth rates of all species are essentially identical. During this period, about 90% of the RNA is present as the inactive 5′-bound enzyme–template complex, the remainder being distributed uniformly over the other intermediates. (4) The decline is free enzyme concentration begins at about 5 min and becomes precipitous at about 10 min. At this time, a gradual transition to the linear growth phase occurs. The growth is never quite linear, however, as the steadily increasing RNA concentration gives ever-increasing inhibition by forming ${}_nIEP_n$ from the reaction ${}_nIE$ + I.

These general features were characteristic of all simulations with symmetric plus and minus strand replication for the starting condition of small amounts of RNA compared to enzyme. There were understandable variations with chain length, rate constants, and concentrations.

The other typical situation investigated in laboratory in vitro experiments is when the RNA and enzyme concentrations are comparable. The dynamic features of the system of differential equations for this starting condition are illustrated in Figures 11–13 for a chain length of 32. The starting amounts of

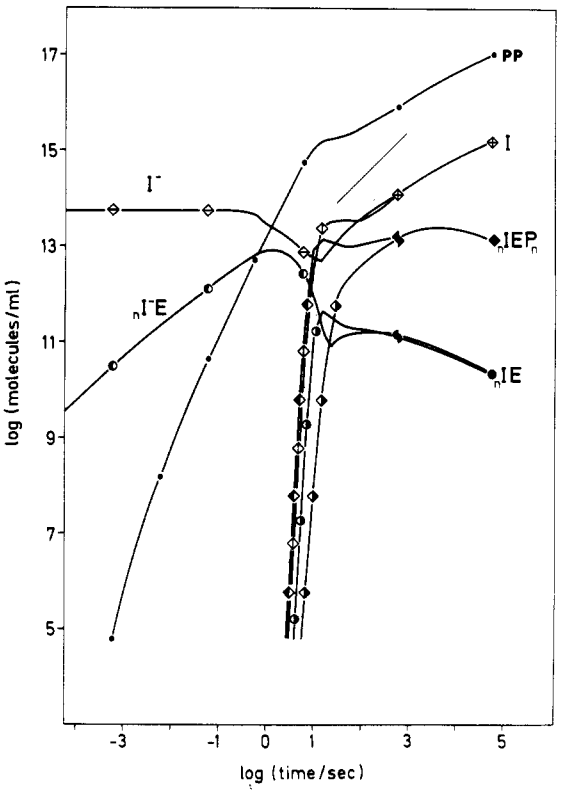

FIGURE 11: Profiles for $n = 32$ and standard set of rate constants except $k_{PI} = 2.5 \times 10^6$. Starting conditions: $[E] = 10^{-7}$ M, $[S_0] = 10^{-4}$ M, $[I^-] = 10^{-7}$ M, all other concentrations zero. Symbols as in Figure 4. The fine line indicates the unit slope corresponding to linear growth of RNA concentration. Half-filled symbols indicate minus (left side filled) and plus (right side filled) strand replication complexes; $[I^+]$ and $[I^-]$ profiles are indicated by vertical and horizontal bars, respectively.

enzyme and substrate were as before, while the starting amounts of RNA were $[I^-] = [E] = 10^{-7}$ M. The following features appear: (1) synthesis of the plus strand begins immediately, while minus strand synthesis is delayed until plus

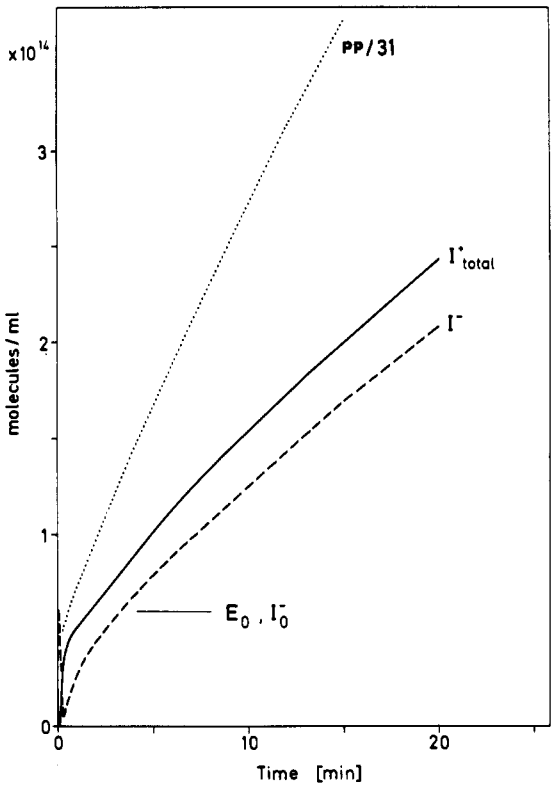

FIGURE 12: Linear growth region at short times for the conditions of Figure 11.

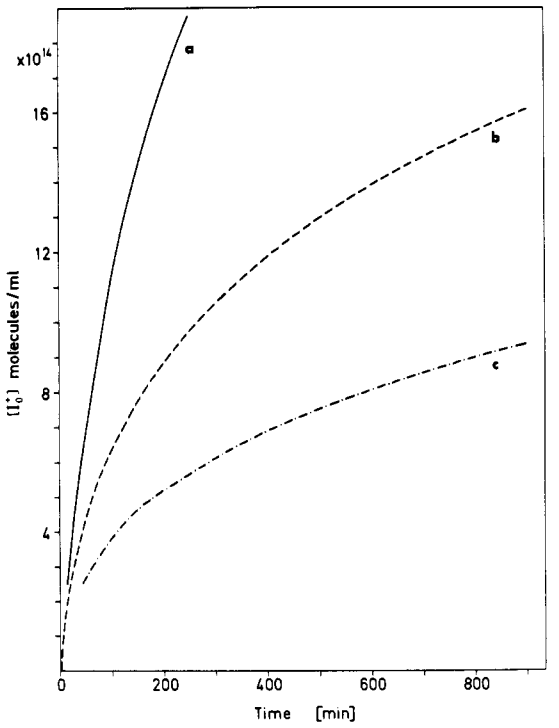

FIGURE 13: Linear growth region at long times for the conditions of Figure 11, showing the effect of varying the product inhibition rate constant. (a) $k_{PI} = 2.5 \times 10^5$; (b) $k_{PI} = 2.5 \times 10^6$; (c) $k_{PI} = 2.5 \times 10^7$.

strands are released to serve as template; (2) the sudden appearance of plus strands at about 10-s reaction time is accompanied by very rapid synthesis of plus strand replication complexes compared to the case shown in Figure 8, leading to sharp oscillations during the transition to linear growth; (3) the profiles for the two strands begin to run together after about 1000-s reaction time; (4) there is again no real period

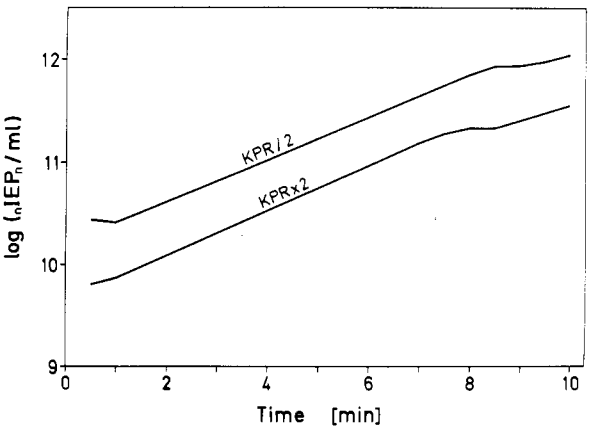

FIGURE 14: Effect of varying k_{PR} on the rate of exponential growth. Conditions as in Figure 5 except $n = 10$.

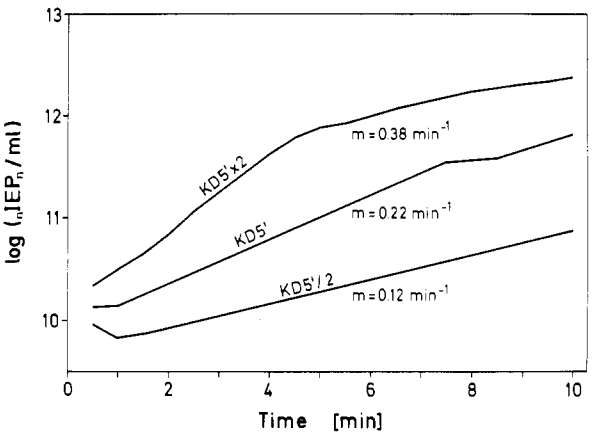

FIGURE 15: Effect of varying $k_{D5'}$ on the rate of exponential growth. Conditions as in Figure 14.

of linear growth, as the effects of product inhibition manifest themselves at the very start of plus strand replication.

A large number of tests with different sets of rate constants were carried out to test the expectations from the theoretical analysis described under Analytical Theory. The rate of exponential growth—albeit not the time required to reach the linear growth phase—indeed proved to be essentially independent of the product (replica) release rate constant, k_{PR}, for the standard set of rate constants, as shown in Figure 14. The exponential growth rate does, however, depend on the rate constant for template release, $k_{D5'}$ (Figure 15).

It was of particular interest to examine the dependence of the exponential growth rate upon the reactivation rate constant, as the relative rates of replica synthesis and enzyme reactivation have important consequences for the rate constants deduced for the exponential and linear phases (see Analytical Theory). For this purpose, we investigated a 100-fold range of reactivation rate constants about the value that represented the laboratory data. This was done for two reactivation models: indirect reactivation, for which $k_{5'3'} = 0$ and $k_{D5'}$ was varied, and direct reactivation, for which $k_{D5'} = 0$ and $k_{5'3'}$ was varied. The result is shown in Figure 16. It can be seen that the theoretically expected linear and square-root dependences are confirmed near the standard values for these rate constants, while stronger and weaker dependences are found for larger deviations.

The simulations described so far were carried out for a uniform set of rate constants for each of the n steps of the elongation process. To test the effects of pause sites on the effective elongation rate, $n = 50$ simulations were carried out in which the entire "time delay" of the elongation (the sum

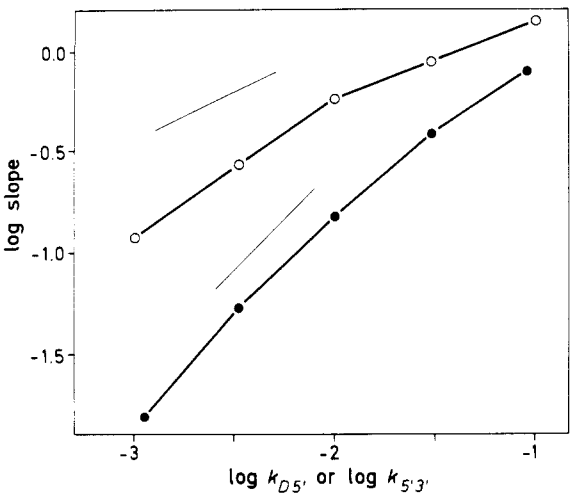

FIGURE 16: Dependence of the slope in the exponential growth region on $k_{D5'}$ (○) and $k_{5'3'}$ (●). The theoretical slopes given by the analytical equations are shown as thin lines. Conditions as in Figure 14.

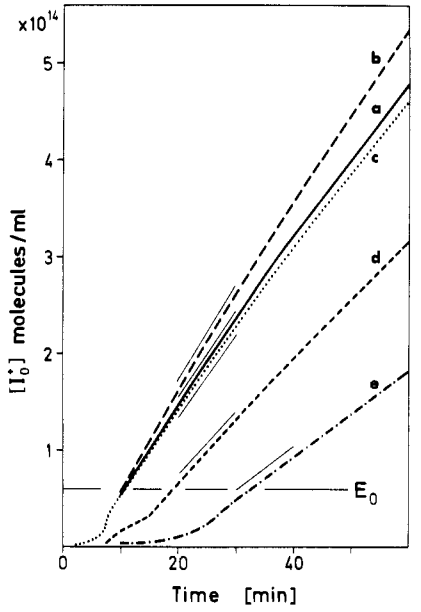

FIGURE 17: Effect of pause sites, $k_{A5'}$, and direct reactivation. Starting conditions as in Figure 8. (a) Standard rate constants, $k_{A5'} = 10^5$; (b) as in (a) except for pause site elongation mechanism (see text); (c) direct reactivation, $k_{D3'} = 0$, $k_{5'3'} = 10^{-2}$ [otherwise as in (a)]; (d) pause sites as in (b) but $k_{A5'} = 10^7$; (e) as (a) except $k_{A5'} = 10^7$.

of the inverse rate constants k_{FP} for all elongation steps) was assigned to the two elongation sites at $j = 16$ and $j = 32$. The results are shown in Figure 17. It can be seen that there is a substantial difference in the synthesis rate in the linear phase for the pause site simulations. It can also be seen that the synthesis rate depends sensitively on the rate constant for product inhibition and that direct reactivation gives a somewhat lower synthesis rate than indirect reactivation.

The effects of having dissimilar rate constants in the plus and minus replication cycles were investigated in the following way. The theoretical analysis (to be presented in a subsequent paper) indicated that unequal rate constants in the two cycles are compensated by concentration adjustments such that concentration ratios become equal to square roots of rate constant ratios (Table II). Simulations were carried out for $n = 50$ using the standard set of rate constants except for $k_{D5'}$, which was multiplied in one cycle and simultaneously divided in the other by factors of 2, 4, and 8. Given a square-root dependence on this rate constant, the concentration ratios

Table IV: Asymmetry Effects[a]

		exponential phase (3 min)			linear phase (30 min)		
factor	$1/\kappa$	$[I_0^+]$	$[I_0^-]$	ratio	$[I_0^+]$	$[I_0^-]$	ratio
1	95	0.026	0.026	1.0	2.7	2.7	1.0
2	92	0.022	0.031	1.5	2.3	2.5	1.1
4	88	0.018	0.037	2.1	1.8	2.2	1.2
8	85	0.016	0.043	2.7	1.3	1.3	1.0

[a] In the exponential phase (at 3 min), $1/\kappa$ (in seconds) was determined from the exponent of the exponential increase of the pyrophosphate concentration. In the linear phase (at 30 min), $1/\kappa$ was determined from the slope of the linear increase of the pyrophosphate concentration. Concentrations are expressed in 10^{14} molecules/cm^3 units.

should then be in these ratios also. The results of the test are shown in Table IV.

The Michaelis-Menten dependence upon substrate concentration indicated by the analytical theory was confirmed by simulations at varying substrate concentration. For the choice of standard rate constants used, Michaelis–Menten behavior was limited to substrate concentrations near K_M; the effect of the initiation rate became apparent for only slightly lower substrate concentrations. The simulations showed the same difficulty of assigning the linear growth rate as did the experiments, in that product inhibition is manifest even in the earliest stages of the linear growth phase.

Discussion

The success of the analytical theory and the computer simulations in accounting for the experimental observations on the kinetics of replication of nonphysiological templates by Qβ replicase is quite satisfying. All phases of the replication process could be described with plausible values for elementary reaction rate constants and reasonable assumptions for deriving analytical expressions. We must still consider the extent to which the conclusions drawn here may be valid for other biochemical information–transfer processes and the implications of our results for validating simpler reaction mechanisms that may be used to describe the kinetics of self-replication in broader contexts, in particular for viral attack on a host cell in vivo and for the self-replication process under selection pressure, i.e., when competition between RNAs with different replication rate constants occurs.

The framework mechanisms presented here may well turn out to be suitable for a general description of single-stranded RNA replication in vitro and possibly also in vivo. Two limitations are apparent. While the total enzyme concentration is constant under laboratory conditions, the enzyme concentration in vivo is a dynamic variable controlled by regulated biosynthesis using the viral genome as message and by spontaneous or enzymic decay. Merely taking the total enzyme concentration as a variable would require only minor extension, and no revision, of the basic (Figure 4) reaction mechanism. The rate characteristics, however, may change drastically. If the enzyme concentration increases in proportion to the template concentration, the system—representing a simple hypercycle—grows hyperbolically (Eigen, 1971; Eigen & Schuster, 1977). It is more likely, however, that one of the two catalytic compounds builds up an excess, which establishes exponential growth conditions. If both compounds can be monitored independently, the coupled rate between them might provide further insight into the mechanism. It is reasonable to suppose that some sort of effective rate constant for translation, valid for specific in vivo conditions only, could be measured by suitable experiments. However, numerous additional complications may arise (Weissmann, 1974).

The second limitation is that the mechanism only describes single-strand replication. Double-stranded viruses, or viruses like influenza that apparently contain more than one RNA species per virus particle, would not have infection kinetics describable by an extension of the mechanism used in this research. For these perhaps far more complex replication processes, the present work can only serve as an encouragement to believe that the traditional methods of chemical kinetics can be applied to biochemical polymerizations in general. Indeed, some of the complications that pertain to the nonphysiological single-stranded templates have also been ignored, e.g., annealing to double strands, metastable tertiary structures, and de novo synthesis.

More direct inferences can be drawn from our results about the nature of the selection process in molecular evolution. While there is an exponential growth phase in the enzyme-excess replication process of evolutionally stable RNA, it is not quite the same as the exponential growth of new mutants in an RNA-excess situation. In the evolutionally stable RNA case, it is a combination of replication and reactivation rates that determines the exponential growth rate; in a competitive situation with RNA in excess, only the (direct or indirect) reactivation rate governs the competition for the enzyme's template site and hence the rate at which a better-adapted (in just this sense) mutant RNA will grow to dominance. However, even in the case of evolutionally stable RNA, there are (with the exception of a really palindromic sequence) two complementary RNA species which might compete with each other. In most experiments involving evolutionally optimized RNA variants produced de novo by Qβ replicase, the amounts of plus and minus strands were found to be approximately equal in both the linear and exponential growth phases. Apparently, it is a characteristic of the optimization process that the net kinetic behavior in each cycle is balanced. There is no obvious chemical reason to believe that this is a strict requirement. We are thus led to inquire what effect different rate constants for the plus and minus replication cycles would have upon the production rates. Extension of the analytical theory and simulations to describe plus/minus asymmetry effects in detail, and to describe competition and evolution of different RNA strands, will be presented in a subsequent paper.

There proved to be, not unexpectedly, a greater number of important rate constants than would be susceptible to laboratory measurement. Many important mechanistic questions cannot be decided by nucleotide incorporation rate measurements alone: the roles of pause sites, the mechanism of direct reactivation, and the details of the initiation mechanism. The analytical expressions thus do not permit connections to be made between RNA production rates and elementary reaction rates without additional information. This information can be provided by a careful analysis of the concentrations of all intermediates since they are related to the residence times calculated in Figure 5. Fast steps will be insufficiently resolved since the concentrations of the corresponding intermediates will be too small. Slow and especially rate-limiting steps, however, are easily recognized and—for the linear growth phase—can be calculated with

$$[I_j] = v/k_j$$

where $1/k_j$ is the residence time for the intermediate I_j and v the overall rate $d[I_0]/dt$. An investigation of the elongation intermediates—which are easy to separate according to their chain lengths—has led to the conclusion that the rate of elongation is determined by a few slow steps (Mills et al., 1978).

It should be noted that the numerical values of the rate parameters obtained refer only to the RNA templates used and can by no means be taken as general values for Qβ replicase. It was found, however, that all optimized RNA variants studied so far (Biebricher et al., 1981a) have similar overall rates and similar rate-limiting steps. In the linear phase and under substrate saturation conditions, the reactivation of the replicase was found to be rate limiting, requiring about 1–2 min. The Michaelis constant determined for RNA variants (Biebricher et al., 1981b) was found to be equal to that for Qβ RNA itself, i.e., 0.2 mM (Mitsunari & Hori, 1973). If in the elongation reaction phosphodiester bond formation is the slowest step ($k_{DSj} \gg k_{FPj}$), the Michaelis constant represents the substrate–enzyme dissociation constant. The values of k_{ASj}/k_{DSj} than fall into a plausible range of rate parameters as have been established for analogous association/dissociation processes. The experimental turnover number per nucleotide incorporated (k_T/n) is in the range of 5–10 s^{-1}. However, the average turnover number and the Michaelis constant values are determined by the few slow elongation steps where additional, slow reactions, e.g., conformation changes of replica and template and strand separation, may be involved. The rate constants associated with these rate-limiting steps are then more likely to be about 0.1 s^{-1}. The "typical" nucleotide incorporation rate may be several orders of magnitude higher [cf. Aivazashvili et al. (1981)], exceeding the above values of k_T/n of 10 s^{-1}. They are thus in a range common for turnover numbers of enzymic reactions.

Our experimental kinetic analysis of RNA replication (Biebricher et al., 1981b) allows the following conclusions to be made: Binding of template with enzyme is strong, the binding constant being significantly larger than 10^7 M^{-1}. Binding of RNA at the replica site—leading to product inhibition—is at least 1 order of magnitude weaker. Geminal association was found to proceed rapidly and was not rate limiting under standard triphosphate concentrations. The rate has not been studied experimentally so far. Since geminal association requires only one substrate, GTP, that furthermore can be replaced in the elongation reaction (but not in the geminal association) by ITP, it can be kinetically separated from elongation by varying the triphosphate concentrations.

Within the described limitations, the theory provides clear guidelines for the interpretation of replication kinetics experiments, as summarized in Table III.

We conclude with a cautionary remark. The apparent simplicity of the system considered in this work might suggest the possible use of Qβ replicase as a general catalyst for amplification of (perhaps suitably modified) RNAs. However, as discussed above, practically all steps of the replication are affected by the secondary and tertiary structure of the template. This property severely restricts the number of primary sequences that will be accepted by the replicase, especially if the rapid evolution and selection of more effectively replicated mutants are taken into account (Briebricher et al., 1981a). The example of Qβ virus itself, on the other hand, proves that it is possible in the evolutionary process to reconcile the manifold structural requirements for replication such that a successful optimized structure results. We note by way of contrast that while the DNA replication system is by far more complicated than the Qβ system, it does—as far as we know today—free the information content of the molecule from any constraint derived from having to be compatible with the replication process.

Supplementary Material Available

An appendix explaining induction period kinetics at early

times (16 pages). Ordering information is given on any current masthead page.

Registry No. RNA replicase, 9026-28-2.

References

Aivazashvili, V. A., Bibilashvili, R. Sh., Vartikyan, R. M., & Kutateladze, T. V. (1981) *Mol. Biol. (Moscow) 15*, 653–667.

Ammann, J., Delius, H., & Hofschneider (1964) *J. Mol. Biol. 10*, 557–561.

August, J. T., Cooper, S., Shapiro, L., & Zinder, N. D. (1963) *Cold Spring Harbor Symp. Quant. Biol. 28*, 95–97.

August, J. T., Banerjee, A. K., Eoyang, L., Franze de Fernandez, M. T., Hori, K., Kuo, C. H., Rensing, U., & Shapiro, L. (1968) *Cold Spring Harbor Symp. Quant. Biol. 33*, 73–81.

Banerjee, A. K., Eoyang, L., Hori, K., & August, J. T. (1967) *Proc. Natl. Acad. Sci. U.S.A. 57*, 986–993.

Banerjee, A. K., Rensing, U., & August, J. T. (1969) *J. Mol. Biol. 45*, 181–193.

Biebricher, C. K., & Orgel, L. E. (1973) *Proc. Natl. Acad. Sci. U.S.A. 70*, 934–938.

Biebricher, C. K., Eigen, M., & Luce, R. (1981a) *J. Mol. Biol. 148*, 369–390.

Biebricher, C. K., Eigen, M., & Luce, R. (1981b) *J. Mol. Biol. 148*, 391–410.

Biebricher, C. K., Diekmann, S., & Luce, R. (1982) *J. Mol. Biol. 154*, 629–648.

Blumenthal, T. (1980) *Proc. Natl. Acad. Sci. U.S.A. 77*, 2601–2605.

Dobkin, C., Mills, D. R., Kramer, F. R., & Spiegelman, S. (1979) *Biochemistry 18*, 2038–2044.

Eigen, M. (1971) *Naturwissenschaften 58*, 465–523.

Eigen, M., & Schuster, P. (1977) *Naturwissenschaften 64*, 541–565.

Eikhom, T. S., & Spiegelman, S. (1967) *Proc. Natl. Acad. Sci. U.S.A. 57*, 1833–1840.

Fedoroff, N. (1975) in *RNA Phages* (Zinder, N., Ed.) pp 235–258, Cold Spring Harbor Laboratory, Cold Spring Harbor, NY.

Feix, G. (1976) *Nature (London) 259*, 593–594.

Feix, G., & Hake, H. (1975) *Biochem. Biophys. Res. Commun. 65*, 503–509.

Feix, G., & Sano, H. (1975) *Eur. J. Biochem. 58*, 59–64.

Feix, G., Slor, H., & Weissmann, C. (1967) *Proc. Natl. Acad. Sci. U.S.A. 57*, 1401–1408.

Feix, G., Pollet, R., & Weissmann, C. (1968) *Proc. Natl. Acad. Sci. U.S.A. 59*, 145–152.

Franklin, R. M. (1966) *Proc. Natl. Acad. Sci. U.S.A. 55*, 1504–1508.

Haruna, I., & Spiegelman, S. (1965a) *Proc. Natl. Acad. Sci. U.S.A. 54*, 579–587.

Haruna, I., & Spiegelman, S. (1965b) *Proc. Natl. Acad. Sci. U.S.A. 54*, 1189–1193.

Haruna, I., & Spiegelman, S. (1965c) *Science (Washington, D.C.) 150*, 884–886.

Haruna, I., Nozu, K., Ohtaka, Y., & Spiegelman, S. (1963) *Proc. Natl. Acad. Sci. U.S.A. 50*, 905–911.

Hindmarsh, A. C. (1980) *Assoc. Comput. Mach., Signum Newsletter 15*, 10–11.

Hirth, L., & Richards, K. E. (1981) *Adv. Virus Res. 26*, 145–199.

Hori, K. L., Eoyang, L., Banerjee, A. K., & August, J. T. (1967) *Proc. Natl. Acad. Sci. U.S.A. 57*, 1790–1797.

Kacian, D. L., Mills, D. R., Kramer, F. R., & Spiegelman, S. (1972) *Proc. Natl. Acad. Sci. U.S.A. 69*, 3038–3042.

Kaerner, H. C., & Hoffmann-Berling, H. (1964) *Nature (London) 202*, 1012–1013.

Kelly, R. B., & Sinsheimer, R. L. (1964) *J. Mol. Biol. 8*, 602–605.

Kelly, R. B., & Sinsheimer, R. L. (1967) *J. Mol. Biol. 29*, 237–241.

Kondo, M., & Weissmann, C. (1972a) *Biochim. Biophys. Acta 259*, 41–49.

Kondo, M., & Weissmann, C. (1972b) *Eur. J. Biochem. 24*, 530–537.

Küppers, B.-O., & Sumper, M. (1975) *Proc. Natl. Acad. Sci. U.S.A. 72*, 2640–2644.

Landers, T. A., Blumenthal, T., & Weber, K. (1974) *J. Biol. Chem. 249*, 5801–5808.

Levisohn, R., & Spiegelman, S. (1968) *Proc. Natl. Acad. Sci. U.S.A. 60*, 866–872.

Levisohn, R., & Spiegelman, S. (1969) *Proc. Natl. Acad. Sci. U.S.A. 63*, 807–811.

Loeb, B. T., & Zinder, N. D. (1961) *Proc. Natl. Acad. Sci. U.S.A. 47*, 282–289.

Meyer, F., Weber, H., & Weissmann, C. (1981) *J. Mol. Biol. 153*, 631–660.

Mills, D. R., Pace, N. R., & Spiegelman, S. (1966) *Proc. Natl. Acad. Sci. U.S.A. 56*, 1778–1785.

Mills, D. R., Peterson, R. L., & Spiegelman, S. (1967) *Proc. Natl. Acad. Sci. U.S.A. 58*, 217–224.

Mills, D. R., Kramer, F. R., & Spiegelman, S. (1973) *Science (Washington, D.C.) 180*, 916–927.

Mills, D. R., Kramer, F. R., Dobkin, C., Nishihara, T., & Spiegelman, S. (1975) *Proc. Natl. Acad. Sci. U.S.A. 72*, 4252–4256.

Mills, D. R., Nishihara, T., Dobkin, C., Kramer, F. R., Cole, P. E., & Spiegelman, S. (1977) in *Nucleic Acid-Protein Recognition* (Vogel, H. J., Ed.) pp 533–547, Academic Press, New York.

Mills, D. R., Dobkin, C., & Kramer, F. R. (1978) *Cell (Cambridge, Mass.) 15*, 541–550.

Mitsunari, Y., & Hori, K. (1973) *J. Biochem. (Tokyo) 74*, 263–271.

Obinata, M., Nasser, D. S., & McCarthy, B. J. (1975) *Biochem. Biophys. Res. Commun. 64*, 640–647.

Pace, N. R., & Spiegelman, S. (1966) *Science (Washington, D.C.) 153*, 64–67.

Palmenberg, A., & Kaesberg, P. (1974) *Proc. Natl. Acad. Sci. U.S.A. 71*, 1371–1375.

Rensing, U., & August, J. T. (1969) *Nature (London) 224*, 853–856.

Rozovskaya, T. A., Chenchik, A. A., & Bibilahsvili, R. Sh. (1981) *Mol. Biol. (Moscow) 15*, 636–652.

Schaffner, W., Rüegg, K. J., & Weissmann, C. (1977) *J. Mol. Biol. 117*, 877–907.

Spiegelman, S., & Doi, R. H. (1963) *Cold Spring Harbor Symp. Quant. Biol. 28*, 109–116.

Spiegelman, S., & Hayashi, M. (1963) *Cold Spring Harbor Symp. Quant. Biol. 28*, 161–181.

Spiegelman, S., Haruna, I., Holland, I. B., Beaudreau, G., & Mills, D. R. (1965) *Proc. Natl. Acad. Sci. U.S.A. 54*, 919–927.

Spiegelman, S., Pace, N. R., Mills, D. R., Levisohn, R., Eikhom, T. S., Taylor, M. M., Peterson, R. L., & Bishop,

D. H. L. (1968) *Cold Spring Harbor Symp. Quant. Biol. 33*, 101–124.
Sumper, M., & Luce, R. (1975) *Proc. Natl. Acad. Sci. U.S.A. 72*, 162–166.
Vourmakis, J. N., Carmichael, G. G., & Efstratiadis, A. (1976) *Biochem. Biophys. Res. Commun. 70*, 774–782.
Weber, H., & Weissmann, C. (1970) *J. Mol. Biol. 51*, 215–224.
Weissmann, C. (1974) *FEBS Lett. (Suppl.) 40*, S10–S18.
Weissmann, C., & Feix, G. (1966) *Proc. Natl. Acad. Sci. U.S.A. 55*, 1264–1268.
Weissmann, C., Simon, L., Borst, P., & Ochoa, S. (1963a) *Cold Spring Harbor Symp. Quant. Biol. 28*, 99–104.
Weissmann, C., Simon, L., & Ochoa, S. (1963b) *Proc. Natl. Acad. Sci. U.S.A. 49*, 407–414.
Weissmann, C., Feix, G., & Slor, H. (1968) *Cold Spring Harbor Symp. Quant. Biol. 33*, 83–100.
Weissmann, C., Billeter, M. A., Goodman, H. M., Hindley, J., & Weber, H. (1973) *Annu. Rev. Biochem. 42*, 303–328.
Winkler-Oswatitsch, R., & Eigen, M. (1979) *Angew. Chem., Int. Ed. Engl. 18*, 20–49.
Young, T. R., & Boris, J. P. (1977) *J. Phys. Chem. 81*, 2424–2427.

Kinetic Characterization of Detergent-Solubilized Sarcoplasmic Reticulum Adenosinetriphosphatase†

D. Kosk-Kosicka,‡ M. Kurzmack, and G. Inesi*

ABSTRACT: Functional characterization of sarcoplasmic reticulum (SR) solubilized with the detergent dodecyl octaethylene glycol monoether ($C_{12}E_8$) was carried out by using both steady-state and rapid kinetic methods, and a comparison with the behavior of the adenosinetriphosphatase (ATPase) in leaky membrane vesicles was obtained. In conditions of maximal solubilization, the monomeric state (M_r 116 000 chain) of the ATPase polypeptide chains was established by comparing their ability to undergo covalent cross-linking in the membranous and solubilized states. The monomeric enzyme retains Ca^{2+}-dependent ATPase activity but is much less stable than the membranous enzyme especially in the presence of low (<1 μM) Ca^{2+} or high (pH 6.0) H^+ concentrations. Protection is afforded by occupancy of high-affinity calcium sites and pH 7.5. Depending on the duration and conditions of exposure to $C_{12}E_8$, the enzyme tends to develop a requirement for higher concentrations of activating Ca^{2+}. It is demonstrated by rapid quench methods that, in analogy to the membranous enzyme, the catalytic mechanism of the solubilized ATPase involves early formation of a phosphorylated enzyme intermediate which then undergoes hydrolytic cleavage and releases P_i. The phosphorylated intermediate can also be formed in the reverse direction of the hydrolytic reaction by exposing the enzyme to P_i in the absence of Ca^{2+} at pH 7.5 and in the presence of dimethyl sulfoxide. Addition of this organic solvent is an absolute requirement for the observation of the P_i reaction in the reverse cycle of the detergent-solubilized enzyme. Dilution with an aqueous medium containing millimolar Ca^{2+} and ADP then allows formation of ATP. In optimal conditions the enzyme retains the same number of catalytic sites as the membranous preparation. Therefore, the detergent does not uncover sites that are latent due to aggregation in the membranous state. Within the 1–100 μM range of ATP concentration, the phosphoenzyme turnover in the solubilized preparation is approximately twice as fast as in leaky vesicles. However, at millimolar ATP concentrations, the phosphoenzyme turnover is similar in both preparations, due to an activating effect of high ATP on the membranous, but not the solubilized, ATPase. In addition to a faster turnover, the solubilized enzyme undergoes a more rapid "switch off" from the calcium-activated state (e.g., loss of its ability to be phosphorylated by ATP) upon removal of calcium with ethylene glycol bis(β-aminoethyl ether)-*N,N,N',N'*-tetraacetic acid.

Sarcoplasmic reticulum (SR) adenosinetriphosphatase (ATPase) is most commonly prepared in the form of vesicular fragments of native membrane. However, it is possible to maintain active enzyme preparations following solubilization with detergents (McFarland & Inesi, 1971; LeMaire et al., 1976a). In some cases, the activity of the solubilized preparations has been attributed to tri- or tetrameric aggregates of the M_r ~116 000 ATPase chains (LeMaire et al., 1976b; LeMaire et al., 1978) and in others to monomeric dispersions of single chains (LeMaire et al., 1976a; Jorgenson et al., 1978; Dean & Tanford, 1978; Moller et al., 1980). Of the several detergents which are available for this purpose, dodecyl octaethylene glycol monoether ($C_{12}E_8$) is the most widely used. Therefore, we have chosen this detergent to study the kinetic behavior of SR ATPase in the solubilized state.

Previous studies on the steady-state activity of SR ATPase solubilized in $C_{12}E_8$ have shown that the enzyme retains basic functional features such as catalysis of ATP hydrolysis and its Ca^{2+} dependence (Dean & Tanford, 1978; Moller et al., 1980). On the other hand, it was reported that the solubilized ATPase does not have the complex dependence on ATP concentration which is manifested by the membranous enzyme. Furthermore, the solubilized ATPase undergoes denaturation following removal of calcium (Moller et al., 1982) and lacks the ability to react with P_i to form the phosphoenzyme in the

† From the Department of Biological Chemistry, University of Maryland Medical School, Baltimore, Maryland 21201. *Received September 15, 1982; revised manuscript received February 23, 1983.* This work was supported by the National Institutes of Health (HL-16607) and the Muscular Dystrophy Association.

‡ Permanent address: Department of Biochemistry of Nervous System and Muscle, Nencki Institute of Experimental Biology, Warsaw, Poland.

0006-2960/83/0422-2559$01.50/0